# Pervasive deformation of an oceanic plate and relationship to large >M$_w$ 8 intraplate earthquakes: The northern Wharton Basin, Indian Ocean

Jacob Geersen[1,2]*, Jonathan M. Bull[1], Lisa C. McNeill[1], Timothy J. Henstock[1], Christoph Gaedicke[3], Nicolas Chamot-Rooke[4], and Matthias Delescluse[4]

[1]University of Southampton, National Oceanography Centre Southampton, European Way, Southampton SO14 3ZH, UK
[2]GEOMAR Helmholtz Centre for Ocean Research Kiel, Wischhofstr. 1-3, 24148 Kiel, Germany
[3]Bundesanstalt für Geowissenschaften und Rohstoffe (BGR), Stilleweg 2, 30655 Hannover, Germany
[4]ENS Laboratoire de Géologie, CNRS UMR8538, PSL Research University, Paris, France

## ABSTRACT

Large-magnitude intraplate earthquakes within the ocean basins are not well understood. The M$_w$ 8.6 and M$_w$ 8.2 strike-slip intraplate earthquakes on 11 April 2012, while clearly occurring in the equatorial Indian Ocean diffuse plate boundary zone, are a case in point, with disagreement on the nature of the focal mechanisms and the faults that ruptured. We use bathymetric and seismic reflection data from the rupture area of the earthquakes in the northern Wharton Basin to demonstrate pervasive brittle deformation between the Ninetyeast Ridge and the Sunda subduction zone. In addition to evidence of recent strike-slip deformation along approximately north-south–trending fossil fracture zones, we identify a new type of deformation structure in the Indian Ocean: conjugate Riedel shears limited to the sediment section and oriented oblique to the north-south fracture zones. The Riedel shears developed in the Miocene, at a similar time to the onset of diffuse deformation in the central Indian Ocean. However, left-lateral strike-slip reactivation of existing fracture zones started earlier, in the Paleocene to early Eocene, and compartmentalizes the Wharton Basin. Modeled rupture during the 11 April 2012 intraplate earthquakes is consistent with the location of two reactivated, closely spaced, approximately north-south–trending fracture zones. However, we find no evidence for WNW-ESE–trending faults in the shallow crust, which is at variance with most of the earthquake fault models.

## INTRODUCTION

The breaking and fracturing of the Indo-Australian plate is a spectacular example of an active diffuse plate boundary within the ocean basins. In the Central Indian Basin, seismic reflection data have imaged compressional faulting and long-wavelength folding with an onset around 15 Ma associated with north-south P axes (Bull and Scrutton, 1992; Chamot-Rooke et al., 1993; Krishna et al., 2001; Delescluse et al., 2008; Bull et al., 2010). In sharp contrast, within the Wharton Basin, east of the Ninetyeast Ridge where the Indo-Australian plate subducts beneath the Sunda plate (Fig. 1A), deformation is predominantly strike slip with northwest-southeast P axes (Petroy and Wiens, 1989; Stein et al., 1989; Delescluse and Chamot-Rooke, 2007). The spatial changes in deformation style are broadly explained by Euler poles that define diffuse plate boundaries between the Indian, Capricorn, and Australian plates (Royer and Gordon, 1997; Bull et al., 2010; Sager et al., 2013).

The Wharton Basin is dissected by long, approximately north-south–trending fossil fracture zones formed at the Wharton Ridge between ca. 36.5 Ma and 83 Ma (Fig. 1A; Deplus et al., 1998; Carton et al., 2014; Jacob et al., 2014). These fracture zones recently attracted attention due to the 11 April 2012 M$_w$ 8.6 and M$_w$ 8.2 strike-slip intraplate earthquakes, which seem to have been promoted by stress transfer following the A.D. 2004 and 2005 Sunda megathrust events (Delescluse et al., 2012). Although modeling of the earthquake sequence is complicated by the absence of remote-sensing and geodetic measurements as well as by the complex faulting scenario, most earthquake models agree that the M$_w$ 8.6 main shock involved rupture on one NNE-SSW–trending and two WNW-ESE–trending faults, with most of the seismic moment released during NNE-SSW rupture (Meng et al., 2012; Wei et al., 2013). The M$_w$ 8.2 aftershock, which occurred two hours later, ruptured a second NNE-SSW–trending fault (Fig. 1; Wei et al., 2013). Due to sparse geophysical data coverage, the basin-wide deformation pattern and its temporal evolution are poorly understood. Here, we discuss multibeam bathymetry and seismic reflection data collected prior to the 2012 earthquakes, extending from the Ninetyeast Ridge to the Sunda Trench in the area that ruptured in the 2012 earthquakes.

## SEISMO-STRATIGRAPHIC INTERPRETATION

The seismic data show three sedimentary units (Fig. 2; see the GSA Data Repository[1]) based on stratigraphic geometry and reflection attributes, with total sediment thickness from 1000 m to >4000 m (see also Geersen et al., 2013). Unit 1 is present only in the central and eastern study area and represents the trench wedge characterized by parallel, high-amplitude reflectors onlapping an unconformity (blue line in Fig. 2) separating units 1 and 2. The distance between the deformation front and the westernmost point of unit 1 combined with the convergence rate between the Indo-Australian and Sunda plates gives an age of ca. 4 Ma (ca. 3.9 Ma, northern transect; ca. 4.3 Ma, southern transects) for the unit 1–unit 2 boundary. Unit 2 is characterized by parallel, high-amplitude reflectors representing Bengal-Nicobar Fan deposits. Buried channels are visible in units 1 and 2. Unit 3 can be distinguished from unit 2 by a low-amplitude reflection pattern, lack of channels, and increased seismic velocity (Singh et al., 2011). The seismic properties of unit 3 and its position directly above the Paleocene oceanic basement suggest it is composed of pelagic sediments. Unit 3 pre-dates Bengal-Nicobar Fan deposition at this latitude, which probably started in the middle Eocene, ca. 40 Ma (Curray et al., 1982). Based on the approximated ages of the unit boundaries (unit 1–unit 2 = ca. 4 Ma; unit 2–unit 3 = ca. 40 Ma), we estimate the ages of seismic horizons assuming constant unit sedimentation rates (see inset table in Fig. 2). These data provide an approximate chronology for the stratigraphy that we believe is sufficient to resolve not only relative fault activity but their absolute slip history. The top of the oceanic basement (TOB) defines the base of unit 3, and is undulating and offset as much as ~900 m by some faults (red arrows in Fig. 2).

---

**359**

Figure 1. A: Overview map of eastern Indian Ocean (data from GEBCO_08 Grid, version 20091120 [www.gebco.net/data _and_products/gridded _bathymetry_data/]). Fracture zones (red solid lines) and Wharton fossil ridge (red dotted lines) after Jacob et al. (2014). Blue lines are faults modeled for the A.D. 2012 intraplate earthquakes (Wei et al., 2013). India (IN)–Australia (AU) relative plate motion from Sager et al. (2013). Focal mechanisms: red are main shocks of the 11 April 2012 intraplate earthquakes; black are aftershocks (until 31 April 2012) (both from International Seismological Centre catalogue, www.isc.ac.uk/iscgem/); green are historic events (A.D. 1897–2005) from Delescluse and Chamot-Rooke (2007). B: Multibeam bathymetric data from study area. Purple (west) and orange (east) lines represent seafloor



lineaments (compare panels C, D, and E), with inset histogram in bottom right corner showing their strike direction. Fracture zones (F6, F7, F8) after Jacob et al. (2014). Black lines indicate locations of seismic transects BGR06-101, 102 (Fig. 2A) and BGR06-103, 104, 105 (Fig. 2B). MD—*MARION-DUFRESNE II*. C–E: Close-ups of multibeam bathymetric data. F: Model of strain for the Wharton Basin with spatial distribution pattern of Riedel shears and north-south fracture zones.
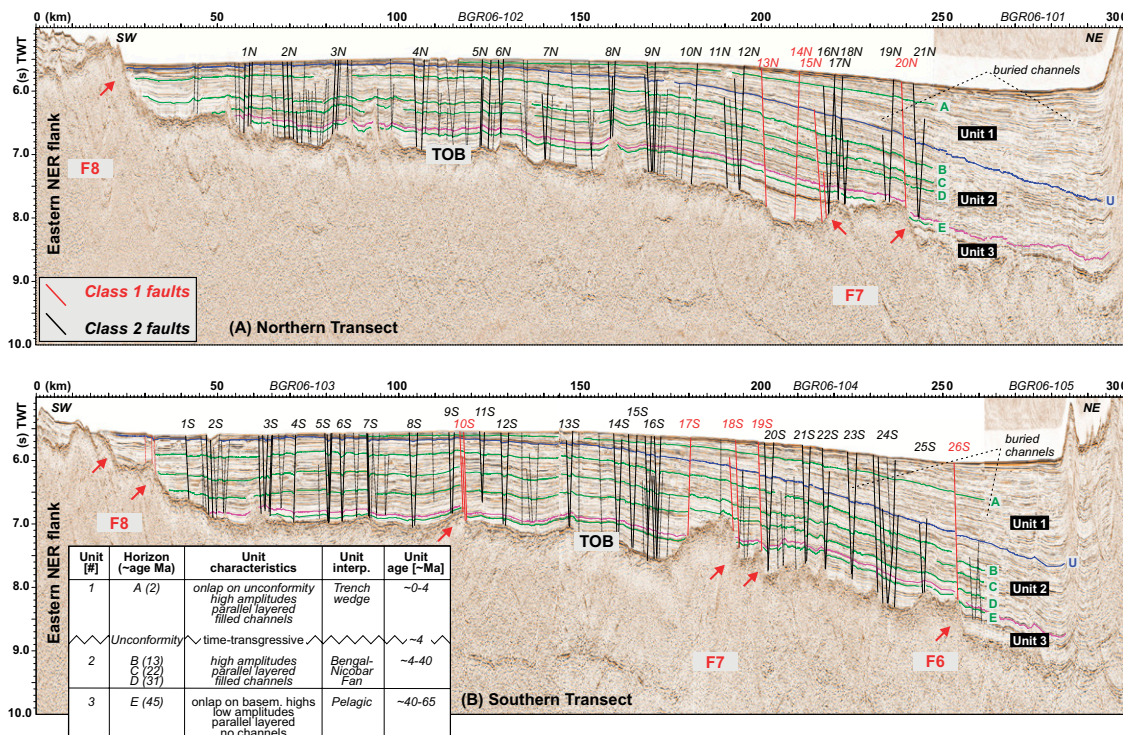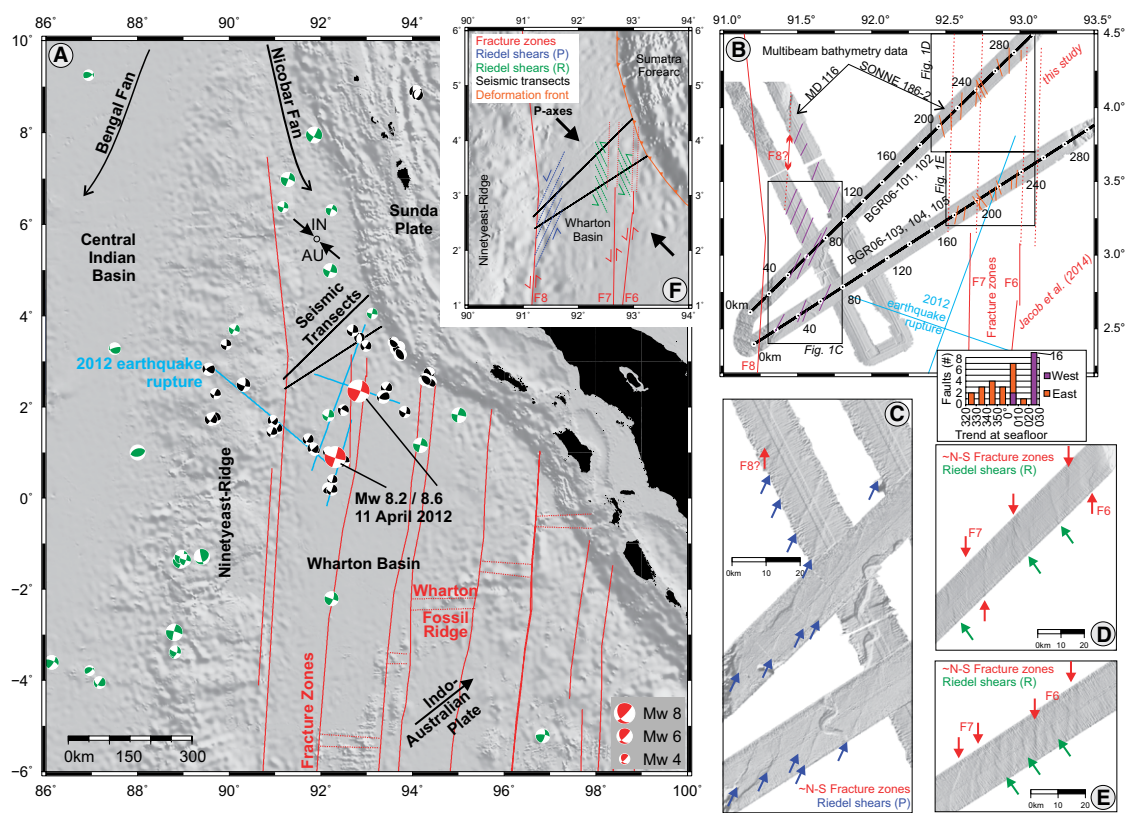


Figure 2. Seismic transects across Wharton Basin (location shown in Fig. 1). Class 1 and class 2 faults are shown by red and black lines, respectively, while horizons used in displacement analysis are shown by green and blue lines. Blue line represents the unconformity that separates units 1 and 2. Red arrows indicate major basement offsets produced by class 1 faults. Pink line marks the unit 2–unit 3 boundary. Table inset provides summary of interpreted stratigraphic units and seismic horizons. TOB—top of oceanic basement; NER—Ninetyeast Ridge; TWT—two-way traveltime; basem.—basement.

# TWO FAULT CLASSES REVEALED BY ANALYSIS OF FAULT DISPLACEMENT

The seismic profiles indicate that the oceanic plate from the Ninetyeast Ridge to the Sunda Trench (~300 km) is actively deforming, with a large number of faults that dip in both along-profile directions (Fig. 2). Obvious fault growth strata are not systematically observed. To investigate temporal and spatial variations in fault activity, we measured the vertical offsets (separations) for six seismic horizons (A, U, B, C, D, and E; see inset table in Fig. 2) across each fault, and depth-converted (seismic velocities: 2.0 km/s for unit 1; 2.6 km/s for unit 2; 3.5 km/s for unit 3; Bull and Scrutton, 1990; Dean et al., 2010; Singh et al., 2011) and normalized the data (Fig. 3). We note that the relative horizontal and vertical components of slip on an individual fault may vary with time, and that horizons used for displacement analysis are not perfectly horizontal. However, we believe that these are minor assumptions and that our analysis gives a robust fault slip history. We exclude faults where seismic horizons could not reliably be identified on both sides, and faults with vertical displacements of <20 ms two-way traveltime (TWT) (excluded faults are plotted as dotted lines in Fig. 2). We use variation in vertical separation and the location of faults relative to proposed fracture zones and basement topography to distinguish between two fault classes (Figs. 2 and 3).

The nine class 1 faults (red lines in Fig. 2) show vertical displacements increasing with depth (Fig. 3A), and offset the TOB by as much as 900 m (red arrows in Fig. 2). In most cases, these faults occur at the edges of blocks of elevated basement topography (Fig. 2), and their locations coincide with the positions of proposed approximately north-south–trending fracture zones (Fig. 1).

The vast majority of faults, those of class 2 (black lines in Fig. 2), show an increase in vertical separation with depth to horizon C, but below this horizon the vertical separation decreases (Fig. 3B). Class 2 faults are evenly distributed across the study area. Commonly they form conjugate structures, consistent with both strike-slip and normal faulting, with the conjugate fault pairs converging downsection at or close to the TOB so that the oceanic basement is not offset.

All faults show a rapid decrease in displacement in unit 1 (Fig. 3). No obvious differences in dip occur between the two fault classes or spatially within the study area; fault dip ranges between 60° and 75° with a mean of 64° (dip calculations assume average velocity of 2.75 km/s, from Dean et al. [2010]).

## FAULT ORIENTATION

Multibeam bathymetry data reveal distinct seafloor lineaments in two areas (Figs. 1B–1E). In the west all lineaments relate to class 2 faults
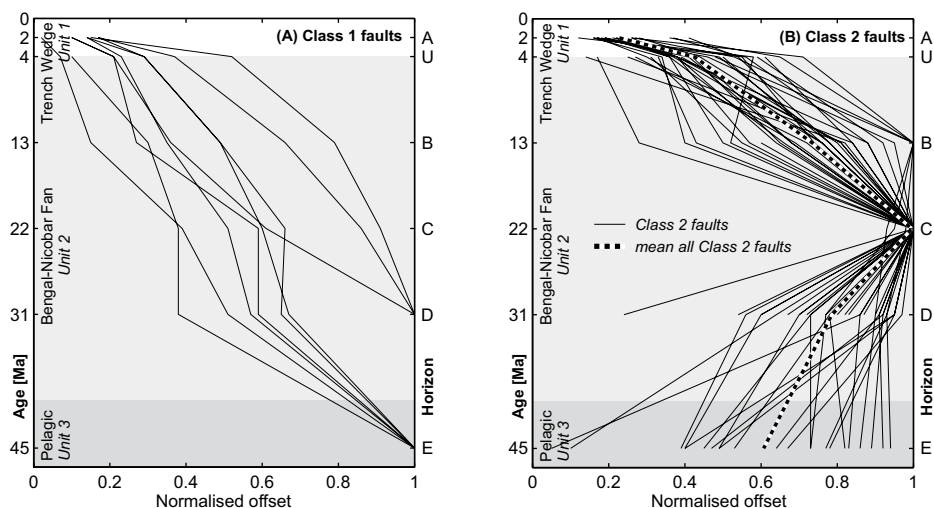


Figure 3. Vertical separation (normalized for each fault by its maximum vertical separation) for all faults marked by solid lines in Figure 2. A: Class 1 faults show continuous increase in vertical separation with depth indicating that they have been continuously active since their formation. B: Class 2 faults show vertical separations that increase with depth down to horizon C before decreasing downward toward top of oceanic basement (TOB).

with consistent northeast-southwest strike direction (020°–030°) (Figs. 1B and 1C). Further east, the strike direction is more heterogeneous, between northwest and northeast (320°–020°) (Figs. 1B, 1D, and 1E), consistent with 000°–015°–trending lineaments and "graben-type features" and smaller structures trending 330°–360° described by Graindorge et al. (2008). There is a correlation between fault class and strike direction: class 1 faults tend to strike approximately north-south (000°–010°) (Figs. 1B, 1D, and 1E); whereas conjugate class 2 faults strike northeast-southwest (020°–030°) close to the Ninetyeast Ridge (Fig. 1C), becoming northwest-southeast trending (320°–360°) close to the subduction zone (Figs. 1D and 1E).

## DISCUSSION

Our structural analysis of the heavily deformed northern Wharton Basin indicates two fault classes with contrasting slip histories. We interpret class 1 faults as the sedimentary-column manifestation of long-lived, left-lateral strike-slip faults that are reactivated approximately north-south–trending fracture zones based on the observations that the faults: (1) do not form conjugate pairs; (2) have constant activity through time, some since the formation of the oceanic crust in the Paleocene; (3) have large vertical basement offsets (up to 900 m); (4) are associated with significant basement topography; and (5) have an orientation of 000°–010°. Following the nomenclature of Singh et al. (2011), fault 26S relates to fracture zone F6, and faults 13N, 14N, 15N, 20N, 17S, 18S, and 19S relate to F7 (Fig. 2). Class 1 fault 10S likely relates to a previously unmapped fracture zone with only a small age offset (J. Dyment, 2015, personal commun.). The consis-

tent increase in vertical displacement with depth for class 1 faults (Fig. 3A), including within stratigraphic unit 3 immediately above oceanic basement, suggests early compartmentalization of the Wharton Basin by fracture zone reactivation from the Paleocene to early Eocene.

We interpret class 2 faults as Riedel faults that form in response to transpression between the reactivated fracture zones. This interpretation is based on: (1) their vertical geometry and extent (conjugate pairs, base close to TOB, no apparent basement offset); (2) their C-shaped vertical displacement profiles; and (3) their strike direction (020°–030° close to the Ninetyeast Ridge and 320°–360° close to the subduction zone) oblique to the approximately north-south fracture zones. Davis et al. (2000) also observed Riedel conjugate shears, associated with left-lateral faults in Utah, not rooted in basement faults. The C-shaped displacement profiles and lack of growth strata indicate that these faults initiated as blind faults at or close to horizon C (maximum displacement) from where they propagated both upwards and downwards (Nicol et al., 1996). The rapid decrease in displacement within unit 1 seems to be controlled by increased sedimentation rates associated with trench wedge deposition rather than fault activity, as this observation is shared by both fault classes (Fig. 3). Class 2 fault deformation is interpreted to have initiated in the Miocene (post–horizon C, ca. 22 Ma) and before deposition of unit 1 (trench wedge, ca. 4 Ma) where a kink in the displacement profiles is observed (Fig. 3). Deformation is ongoing, indicated by most faults extending to the seafloor (Fig. 2).

Graindorge et al. (2008) analyzed multibeam bathymetric and 3.5 kHz seismic data from close to the subduction zone, and described similar northwest-southeast–trending seafloor

structures, interpreted as surface expression of bending-related normal faults. However, the seismic lines presented here demonstrate that the northwest-southeast–trending structures relate to underlying conjugate fault pairs with a C-shaped vertical displacement profile that are ubiquitous across the northern Wharton Basin and that we therefore interpret as Riedel faults.

Comparing our structural analysis, i.e., the location of the approximately north-south–trending fossil fracture zones at the location of the seismic transects, with the modeled rupture of the 2012 intraplate earthquakes (Fig. 1), there is evidence that fracture zones F6 and/or F7 may have ruptured during the events. Many of the published earthquake models show rupture on multiple NNE-SSW– and WNW-ESE–trending faults (Fig. 1A). However, there is no evidence for WNW-ESE faults at the seafloor in our data (Fig. 1). This is most likely because the earthquake rupture on these WNW-ESE faults did not propagate upwards into the overlying sediments, although we acknowledge that the marine geophysical data were collected before the 2012 events.

The main structures described here yield a single coherent model of strain in the Wharton Basin (Fig. 1F). Relative plate motions generate northwest-southeast–oriented P axes, compatible with the left-lateral reactivation of approximately north-south–trending fracture zones (e.g., Delescluse and Chamot-Rooke, 2007). Furthermore, conjugate Riedel shears restricted to the sedimentary column develop between the fracture zones in response to transpression. We infer that the Riedel shears close to the Ninetyeast Ridge are P shears, whereas further east they are R shears. The reason for the dominance of P versus R shear deformation with distance from the Ninetyeast Ridge could be rotation of compressive stress to more north-south (Delescluse and Chamot-Rooke, 2007), or that the faults to the west are older, with scarps preserved due to reduced sedimentation close to the Ninetyeast Ridge (Fig. 2), reflecting more evolved deformation (R shears typically appear first, followed by P shears; Tchalenko, 1970). Due to the uncertainties in our age estimates, we are unable to derive the exact timing, and hence the driving mechanism, for the initiation of Riedel shears. Within the central Indian Ocean, kinematic modeling and seismic reflection data integrated with borehole data showed the onset of diffuse deformation at ca. 15 Ma, with intensification at ca. 8 Ma (e.g., Bull et al., 2010) potentially linked to changes in Himalayan uplift and/or deformation. Future ocean drilling may confirm whether the Riedel shears are of similar age.

## ACKNOWLEDGMENTS

## REFERENCES CITED

Bull, J.M., and Scrutton, R.A., 1990, Sediment velocities and deep structure from wide-angle reflection data around Leg 116 sites, *in* Proceedings of the Ocean Drilling Program, Scientific Results, Volume 116: College Station, Texas, Ocean Drilling Program, p. 311–316.

Bull, J.M., and Scrutton, R.A., 1992, Seismic reflection images of intraplate deformation, central Indian Ocean, and their tectonic significance: Journal of the Geological Society, v. 149, p. 955–966, doi:10.1144/gsjgs.149.6.0955.

Bull, J.M., DeMets, C., Krishna, K.S., Sanderson, D.J., and Merkouriev, S., 2010, Reconciling plate kinematic and seismic estimates of lithospheric convergence in the central Indian Ocean: Geology, v. 38, p. 307–310, doi:10.1130/G30521.1.

Carton, H., Singh, S.C., Hananto, N.D., Martin, J., Djajadihardja, Y.S., Udrekh, Franke, D., and Gaedicke, C., 2014, Deep seismic reflection images of the Wharton Basin oceanic crust and uppermost mantle offshore Northern Sumatra: Relation with active and past deformation: Journal of Geophysical Research, v. 119, p. 32–51, doi:10.1002/2013JB010291.

Chamot-Rooke, N., Jestin, F., and de Voogd, B., 1993, Intraplate shortening in the central Indian Ocean determined from a 2100-km-long north-south deep seismic reflection profile: Geology, v. 21, p. 1043–1046, doi:10.1130/0091-7613(1993)021<1043:ISITCI>2.3.CO;2.

Curray, J.R., Emmel, F.J., Moore, D.G., and Russel, W.R. 1982. Structure, tectonics, and geological history of the northeastern Indian Ocean, *in* Nairn, A.E., and Stheli, F.G., eds., The Ocean Basins and Margins, Volume 6, The Indian Ocean: New York, Plenum, p. 399–450.

Davis, G.H., Bump, A.P., García, P.E., and Ahlgren, S.G., 2000, Conjugate Riedel deformation band shear zones: Journal of Structural Geology, v. 22, p. 169–190, doi:10.1016/S0191-8141(99)00140-6.

Dean, S.M., McNeill, L.C., Henstock, T.J., Bull, J.M., Gulick, S.P.S., Austin, J.A., Bangs, N.L.B., Djajadihardja, Y.S., and Permana, H., 2010, Contrasting décollement and prism properties over the Sumatra 2004–2005 earthquake rupture boundary: Science, v. 329, p. 207–210, doi:10.1126/science.1189373.

Delescluse, M., and Chamot-Rooke, N., 2007, Instantaneous deformation and kinematics of the India–Australia Plate: Geophysical Journal International, v. 168, p. 818–842, doi:10.1111/j.1365-246X.2006.03181.x.

Delescluse, M., Montési, L.G.J., and Chamot-Rooke, N., 2008, Fault reactivation and selective abandonment in the oceanic lithosphere: Geophysical Research Letters, v. 35, L16312, doi:10.1029/2008GL035066.

Delescluse, M., Chamot-Rooke, N., Cattin, R., Fleitout, L., Trubienko, O., and Vigny, C., 2012, 2012 intra-oceanic seismicity off Sumatra boosted by the Banda-Aceh megathrust: Nature, v. 490, p. 240–244, doi:10.1038/nature11520.

Deplus, C., Diament, M., Hébert, H., Bertrand, G., Dominguez, S., Dubois, J., Malod, J., Patriat, P., Pontoise, B., and Sibilla, J.-J., 1998, Direct evidence of active deformation in the eastern Indian oceanic plate: Geology, v. 26, p. 131–134, doi: 10.1130/0091-7613(1998)026<0131:DEOADI>2.3.CO;2.

Geersen, J., McNeill, L., Henstock, T.J., and Gaedicke, C., 2013, The 2004 Aceh-Andaman Earthquake: Early clay dehydration controls shallow seismic rupture: Geochemistry Geophysics Geosystems, v. 14, p. 3315–3323, doi:10.1002/ggge.20193.

Graindorge, D., et al., 2008, Impact of lower plate structure on upper plate deformation at the NW Sumatran convergent margin from seafloor morphology: Earth and Planetary Science Letters, v. 275, p. 201–210, doi:10.1016/j.epsl.2008.04.053.

Jacob, J., Dyment, J., and Yatheesh, V., 2014, Revisiting the structure, age, and evolution of the Wharton Basin to better understand subduction under Indonesia: Journal of Geophysical Research, v. 119, p. 169–190, doi:10.1002/2013JB010285.

Krishna, K.S., Bull, J.M., and Scrutton, R.A., 2001, Evidence for multiphase folding of the central Indian Ocean lithosphere: Geology, v. 29, p. 715–718, doi:10.1130/0091-7613(2001)029<0715:EFMFOT>2.0.CO;2.

Meng, L., Ampuero, J.P., Stock, J., Duputel, Z., Luo, Y., and Tsai, V.C., 2012, Earthquake in a maze: Compressional rupture branching during the 2012 $M_w$ 8.6 Sumatra earthquake: Science, v. 337, p. 724–726, doi:10.1126/science.1224030.

Nicol, A., Watterson, J., Walsh, J.J., and Childs, C., 1996, The shapes, major axis orientations and displacement patterns of fault surfaces: Journal of Structural Geology, v. 18, p. 235–248, doi:10.1016/S0191-8141(96)80047-2.

Petroy, D.E., and Wiens, D.A., 1989, Historical seismicity and implications for diffuse plate convergence in the northeast Indian Ocean: Journal of Geophysical Research, v. 94, p. 12,301–12,319, doi:10.1029/JB094iB09p12301.

Royer, J.-Y., and Gordon, R.G., 1997, The motion and boundary between the Capricorn and Australian plates: Science, v. 277, p. 1268–1274, doi:10.1126/science.277.5330.1268.

Sager, W.W., Bull, J.M., and Krishna, K.S., 2013, Active faulting on the Ninetyeast Ridge and its relation to deformation of the Indo-Australian plate: Journal of Geophysical Research, v. 118, p. 4648–4668, doi:10.1002/jgrb.50319.

Singh, S.C., Carton, H., Chauhan, A.S., Androvandi, S., Davaille, A., Dyment, J., Cannat, M., and Hananto, N.D., 2011, Extremely thin crust in the Indian Ocean possibly resulting from plume–ridge interaction: Geophysical Journal International, v. 184, p. 29–42, doi:10.1111/j.1365-246X.2010.04823.x.

Stein, C.A., Cloetingh, S., and Wortel, R., 1989, Seasat-derived gravity constraints on stress and deformation in the northeastern Indian Ocean: Geophysical Research Letters, v. 16, p. 823–826, doi:10.1029/GL016i008p00823.

Tchalenko, J.S., 1970, Similarities between shear zones of different magnitudes: Geological Society of America Bulletin, v. 81, p. 1625–1640, doi:10.1130/0016-7606(1970)81[1625:SBSZOD]2.0.CO;2.

Wei, S., Helmberger, D., and Avouac, J.-P., 2013, Modeling the 2012 Wharton Basin earthquake off Sumatra: Complete lithospheric failure: Journal of Geophysical Research, v. 118, p. 3592–3609, doi:10.1002/jgrb.50267.

# Geology

## Pervasive deformation of an oceanic plate and relationship to large >$M_W$ 8 intraplate earthquakes: The northern Wharton Basin, Indian Ocean

Jacob Geersen, Jonathan M. Bull, Lisa C. McNeill, Timothy J. Henstock, Christoph Gaedicke, Nicolas Chamot-Rooke and Matthias Delescluse

---

---

**Notes**

THE
GEOLOGICAL
SOCIETY
OF AMERICA